Fusion Engineering and Design 88 (2013) 3060–3071

Contents lists available at ScienceDirect

Fusion Engineering and Design

journal homepage: www.elsevier.com/locate/fusengdes

Experimental and numerical studies of pressure drop in PbLi flows in a circular duct under non-uniform transverse magnetic field

F.-C. Li*, D. Sutevski, S. Smolentsev, M. Abdou

Fusion Science & Technology Center, University of California, Los Angeles, USA

HIGHLIGHTS

- An indirect DP measurement approach for high-temperature LM MHD flow is developed.
- Experiments and numerical simulations of PbLi MHD flow are performed.
- Characteristics of DP in LM MHD flow under fringing magnetic field are studied.
- Pressure distributions in LM MHD flow at entry and exit of magnet are different.

ARTICLE INFO

Article history:
Received 2 April 2013
Received in revised form 8 August 2013
Accepted 8 August 2013
Available online 7 September 2013

Keywords:
Magnetohydrodynamics
Fringing magnetic field
MHD experiment
Numerical simulation
Lead-lithium

ABSTRACT

Experiments and three-dimensional (3D) numerical simulations are performed to investigate the magnetohydrodynamic (MHD) characteristics of liquid metal (LM) flows of molten lead-lithium (PbLi) eutectic alloy in an electrically conducting circular duct subjected to a transverse non-uniform (fringing) magnetic field. An indirect measurement approach for differential pressure in high temperature LM PbLi is first developed, and then detailed data on pressure drop in this PbLi MHD flow are measured. The obtained experimental results for the pressure distribution are in good agreement with numerical simulations. Using the numerical simulation results, the 3D effects caused by fringing magnetic field on the LM flow are illustrated via distributions for the axial pressure gradients and transverse pressure differences. It has been verified that a simple approach for estimation of pressure drop in LM MHD flow in a fringing magnetic field proposed by Miyazaki et al. [22] i.e., a simple integral of pressure gradient along the fringing field zone using a quasi-fully-developed flow assumption, is also applicable to the conditions of the present experiment providing the magnetic interaction parameter is large enough. Furthermore, for two different sections of the LM flow at the entry to and at the exit from the magnet, it is found that the pressure distributions in the duct cross sections in these two regions are different.

Published by Elsevier B.V.

1. Introduction

The concept of a liquid metal (LM) breeding blanket for fusion reactors has advantages of both high thermal efficiency and immunity of LM to irradiation damage compared to solid breeders. Compared to pure lithium, the eutectic alloy lead-lithium (PbLi) has some advantages as a tritium breeder and/or coolant because of its lower chemical reactivity with air, water, and concrete. Typical examples of liquid breeder blankets using PbLi include the dual-coolant lead-lithium (DCLL) [1], helium-cooled lead-lithium (HCLL) [2], self-cooled lead lithium (HCLL) [1], and water cooled lithium-lead (WCLL) blankets [3].

The use of PbLi in the liquid blankets of fusion devices, however, will involve materials and magnetohydrodynamic (MHD) related issues, which are among the most important considerations in any PbLi blanket concept. Although molten PbLi has lower chemical reactivity, it is corrosive to structural steels at high temperatures under fusion conditions. The corrosive nature of molten PbLi, together with other factors such as its opaqueness and the high temperature, may also cause some additional difficulties to hydrodynamic diagnostics (velocity and pressure distributions) of PbLi flows. For magnetically confined fusion reactors, the strong magnetic field used for confinement of the fusion plasma will induce tremendous pressure drops and redistribution of the liquid PbLi flows used in liquid breeder blankets. On the other hand, changes in the PbLi flow caused by MHD effects will also influence material interfaces. For example, the redistributed velocity profile within the cross-section of a flow passage, induced by MHD effects, may result in an altered corrosion rate for high-temperature PbLi flows in steel ducts.

Since the 1980s, tens of experimental facilities utilizing PbLi as a working fluid have been constructed and successfully operated

* Corresponding author.
E-mail addresses: lifch@hit.edu.cn, lifch@fusion.ucla.edu (F.-C. Li).

0920-3796/$ – see front matter. Published by Elsevier B.V.
http://dx.doi.org/10.1016/j.fusengdes.2013.08.006

all over the world [4–10]. Using these facilities, many experimental studies, with and without MHD effects, were conducted. PbLi online monitoring, impurity control and removal [5,11], corrosion behavior of steels by high temperature PbLi [4,7,8,11–16], chemical interaction behaviors between liquid PbLi with oxygen-containing gases and water [17–19], and more became well understood. Nevertheless, there are still many unsolved practical as well as fundamental problems associated with molten PbLi flows in the environment of magnetically confined fusion devices. To address such problems, a MHD PbLi loop has recently been constructed at University of California, Los Angeles (UCLA) [10]. Currently, this loop serves three main purposes: (1) development of diagnostics approaches for high-temperature MHD PbLi flows; (2) demonstration of the performance characteristics of various electrical insulation techniques to reduce the MHD pressure drop; and (3) study of the corrosion behavior of structural steels exposed to high-temperature MHD PbLi flows. All of these experimental studies are also supplemented by numerical simulations.

In this paper, we investigate the characteristics of PbLi flow in an electrically conducting circular duct under a transverse non-uniform magnetic field both experimentally and numerically. For electrically conducting fluid flow in a circular duct interacting with a non-uniform magnetic field, some studies have been performed to investigate flow characteristics from different viewpoints. In [20,21], investigations of MHD flows of a liquid sodium-potassium (NaK) eutectic alloy in a circular duct near the entrance to the magnetic field were carried out experimentally and analytically. Pressure drop, axial pressure gradient, pressure difference between the walls parallel and perpendicular to the magnetic field in a cross section of the flow passage in the fringing region of the magnetic field and velocity distributions were measured. Numerical simulation results of those parameters are also illustrated. In these studies, the three-dimensional (3D) effect caused by the transverse magnetic field on LM flow is demonstrated. In [22], measurements of MHD pressure drop in LM NaK flows in a circular duct under non-uniform transverse magnetic field and an approach to scale the MHD pressure drop data in the fringing region of the applied magnetic field through a simple integral of the pressure gradient are reported. In numerical simulations of LM flows in a circular duct under a strong fringing magnetic field [23], the efficiency of the so-called core flow approximation in modeling LM flows subjected to intense magnetic fields was evaluated after verifying the numerical simulation method and demonstrating the general flow characteristics. In a validation study of numerical simulation methods for LM flow with strong MHD effects [24], fully 3D simulations were performed at UCLA for a circular pipe flow under the same conditions used in the experiments in [20]. Excellent agreements in pressure gradient, transverse pressure difference between the walls parallel and perpendicular to the magnetic field in a cross section and velocity profile were obtained. The numerical simulation code validated in [24], called HIMAG, is used in this study.

The present paper has two purposes. One is to further validate the recently proposed differential pressure measurement approach [10] for pressure measurements in high-temperature (above 300 °C) liquid metals. The second is to comprehensively investigate the effect of the fringing magnetic field on MHD LM flow characteristics. An indirect measurement approach for pressure drop in high temperature PbLi MHD flow used in the study is accompanied with theoretical analyses for inherent measurement error and factors affecting accuracy. The reliability of this approach is verified by comparing the measured data of MHD pressure drop with theoretical analyses for LM MHD pipe flows. The 3D effects of a transverse fringing magnetic field on the characteristics of MHD LM flows are illustrated with the axial pressure gradient profiles taken at the sections of the wall parallel and perpendicular to the magnetic field. Furthermore, based on the numerical computations, the non-uniform fluid pressure distributions in the cross section of the flow passage in the fringing magnetic field are surprisingly found to be different for the two cases of LM flowing into and out the magnetic field.

2. Problem description

We are investigating LM PbLi flow in a conducting circular duct at the entrance to and exit from a transverse magnetic field. In the experiments, only flows entering the magnetic field region are studied, while numerical simulations are performed for both flows entering and leaving the magnetic field region. The flow geometry and distribution of magnetic field are shown in Fig. 1 schematically. LM PbLi flows in a stainless steel tube from left to right and first enters and then leaves a transverse magnetic field. The magnetic field region has a total length of 2 m in the streamwise direction, with a 0.8-m uniform magnetic field length in the center and a 0.6-m fringing field section at each end. The front edges

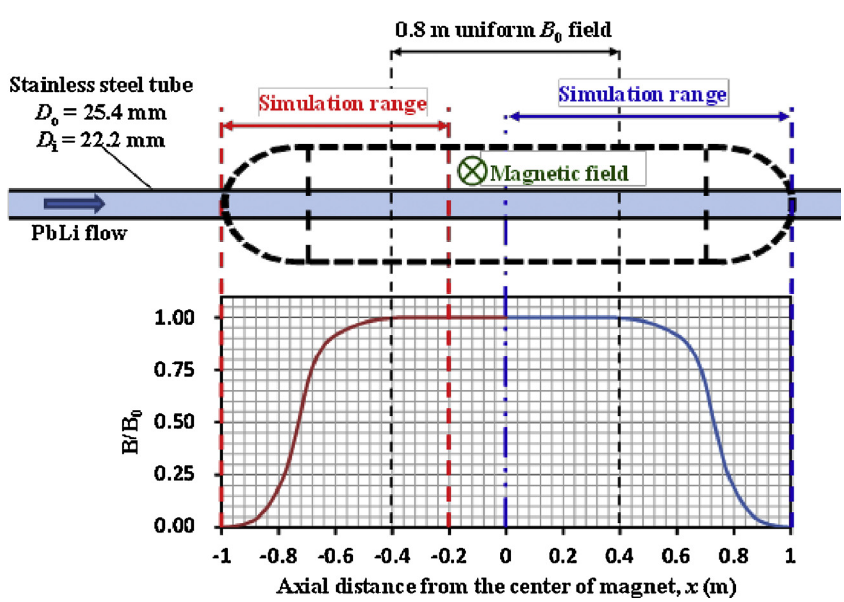

Fig. 1. Schematic diagram showing the flow geometry and distribution of the magnetic field.

of the magnet pole are at $x = \pm 0.7$ m according to the coordinate system plotted in Fig. 1. The MHD LM PbLi flow influenced by the fringing magnetic field at the entrance region is a focus of both experiments and numerical simulations. At the entrance region, the fringing magnetic field distribution used in numerical simulations is obtained by matching the measured values for the magnet used in the experiment [25], as shown in Eq. (1):

$$\frac{B}{B_0} = 0.5 \times [1 + \tanh(10x + 7.315)], \quad -1.0\,m \le x \le -0.4\,m, \tag{1}$$

where B is the local magnetic field, B_0 is the magnetic field in the uniform region and x is the axial distance also shown in Fig. 1. The other, axial, component of the magnetic field was evaluated based on the constraint of the curl-free magnetic field. However, this component is small such that full computations, including two magnetic field components, have demonstrated a negligible effect of the axial field component on pressure drops in the flow for several typical cases that cover the parameter range in the present study. Therefore, most of the computations were performed using only the transverse field component as shown in Eq. (1). For numerical simulations of PbLi flow leaving the magnetic field region, the fringing magnetic field distribution at the exit region is a mirror image of the field distribution at the entrance region.

The governing equations for MHD flow of electrically conducting fluid can be written in the inductionless approximation as follows:

$$\nabla \cdot \mathbf{u} = 0, \tag{2}$$

$$\frac{\partial \mathbf{u}}{\partial t} + \mathbf{u} \cdot \nabla \mathbf{u} = \frac{1}{\rho}(-\nabla p + \nabla \cdot (\eta \nabla \mathbf{u}) + (\mathbf{J} \times \mathbf{B})), \tag{3}$$

$$\mathbf{J} = \sigma(-\nabla \varphi + \mathbf{u} \times \mathbf{B}), \tag{4}$$

$$\nabla \cdot (\sigma \nabla \varphi) = \nabla \cdot (\sigma \mathbf{u} \times \mathbf{B}). \tag{5}$$

Here, $\mathbf{u}$ is the velocity vector, p the pressure, $\mathbf{J}$ the induced current density vector, $\mathbf{B}$ the applied magnetic field vector, φ the electric potential, σ the electrical conductivity, ρ the fluid density and η the fluid dynamic viscosity. The Reynolds number Re, the Hartmann number Ha and the magnetic interaction parameter N are defined as $Re = \frac{\rho R_i U}{\eta}$, $Ha = B_0 R_i \sqrt{\frac{\sigma_f}{\eta}}$ and $N = \frac{Ha^2}{Re} = \frac{\sigma_f B_0^2 R_i}{\rho U}$, respectively, where R_i is the inner radius of the circular duct, U is the bulk velocity and σ_f is electrical conductivity of the fluid.

In the experiments, the flow diagnostics are limited to pressure measurements, made in both the fringing and uniform field regions. In order to elucidate effects of the fringing field on the MHD flow, numerical simulations are then performed to obtain the details of velocity and induced electric current fields. The simulated region is a 0.8-m long circular duct as indicated in Fig. 1. Along the duct, a transverse magnetic field, including the 0.6-m long fringing field and the 0.2-m long uniform field B_0 as described by Eq. (1), is applied.

3. Experimental procedures

3.1. MaPLE loop

The experiments were carried out in a MHD PbLi flow loop [10] named MaPLE (Magnetohydrodynamic PbLi Experiment), as shown in Fig. 2 schematically. The main components of MaPLE facility include an electromagnet, an electromagnetic (EM) pump, an EM flow meter, a flow circuit, a temperature control system (power supplies, heaters, and insulation), and a data sampling system (the last two are not shown in Fig. 2). The electromagnet has a maximum magnetic field of 1.8 T. The flow circuit is composed of a PbLi melting/storage tank and pipelines made of stainless steel SUS304. For the present experiments, the circular duct test section made of stainless steel SUS304 has an outer diameter $D_o = 0.0254$ m and an inner diameter $D_i = 0.0222$ m. A glove box is connected to the melting/storage tank for environment regulation. All the main components sit on a four-wheel carrier so that the whole apparatus can be moved forward or backward easily, facilitating loop maintenance and experimental operations. The presently used PbLi alloy is supplied by Atlantic Metals & Alloys, Inc., USA. The operation fluid temperature is 300 °C. More details of the MaPLE facility are given in [10].

3.2. Pressure drop measurement approach for high-temperature PbLi MHD flow

In this study, we use the differential pressure measurement technique such that a pressure difference is measured between two pressure ports mounted on the top of the horizontal test section as shown in Fig. 3. For liquid PbLi flow, both the high temperature itself and corrosive effects of molten PbLi on metallic materials make it difficult to utilize commercial

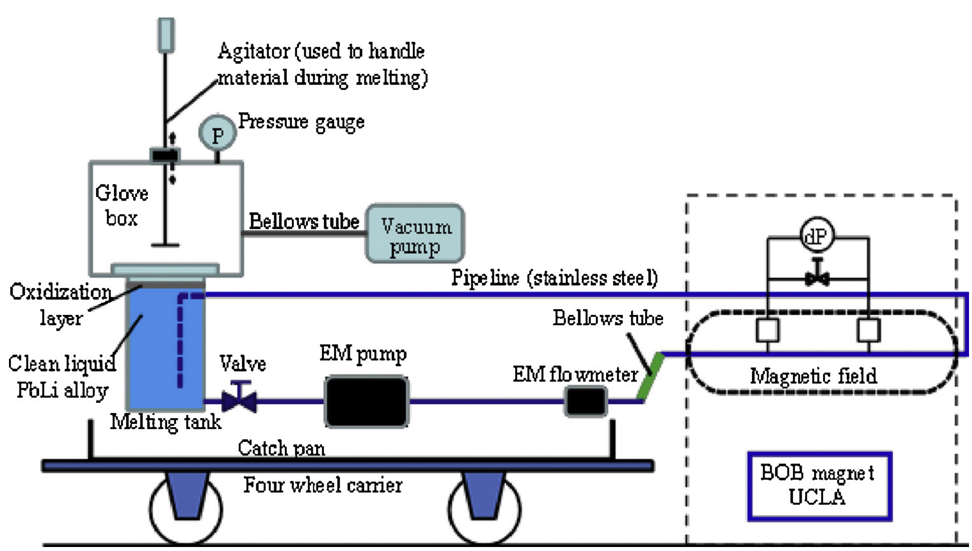

Fig. 2. Schematic diagram of the MHD PbLi loop MaPLE.

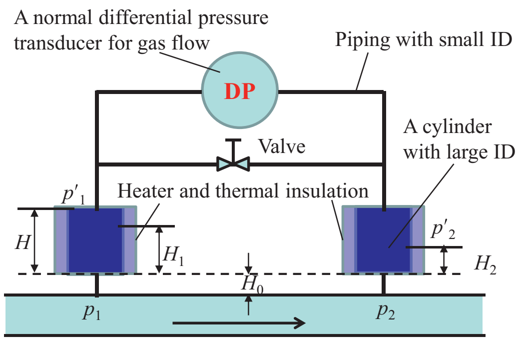

Fig. 3. Schematic of pressure difference measurement sub-loop for high temperature liquid PbLi flow using a normal DP sensor for gas flow.

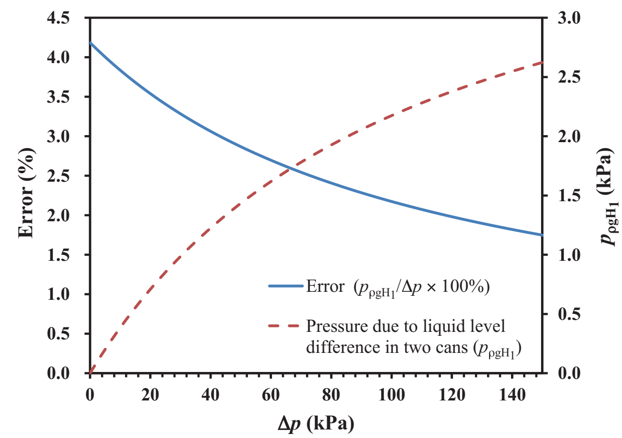

Fig. 4. The estimated error for the indirect DP-measurement system as a function of measured pressure drop.

pressure or differential pressure (DP) transducers in direct contact with the flow. It may cause damage to transducers if high temperature liquid PbLi directly contacts with the diaphragm of a standard pressure or DP sensor. We then developed a measurement approach for mean pressure drop in a high-temperature MHD PbLi flow using a standard DP transducer in an indirect way. The presently used DP sensor is a DP-15 (DP15-40) transducer for gas flows provided by Validyne Engineering Corporation. It has 86 kPa maximum range with ±0.25% accuracy. The DP measurement system is a sub-loop filled with argon gas as schematically shown in Fig. 3 and also in Fig. 2. As seen in Fig. 3, the key feature of this sub-loop is the inclusion of the two identical buffer tanks made of stainless steel with large diameter (D_{it} = 0.0732 m was used herein) and small height (H = 0.047 m) in both the upstream and downstream legs. The other parts of these two buffer tanks are stainless steel pipe lines with much smaller diameter than that of the buffer tanks (a combination of D_{ip1} = 0.00076 m and D_{ip2} = 0.0014 m was used herein). The volume of the thin pipe lines of each leg is much smaller than that of the buffer tanks. Accordingly, the argon gas volume change in each leg of the sub-loop caused by liquid ingress driven by the pressure in the LM flow loop can be limited within the buffer tank according to the thermodynamics theory $pV = constant$ (where V is argon gas volume in each leg). Consequently, the difference between liquid levels in both legs of the DP-measurement sub-loop can be kept small due to the small height of the buffer tank, and the reading from DP sensor can substitute for the real pressure difference $p_1 - p_2$ with an acceptable accuracy, as schematically shown in Fig. 3.

The maximum working temperature of the applied DP-15 transducer is 121 °C, but natural cooling can easily satisfy this temperature limit by exposing the pipe lines, including the DP transducer, over the buffer cylinders in the air. Note that there will be no practical upper temperature limitation of the LM flow to be measured for this indirect DP measurement approach since it prevents the DP transducer diaphragm from directly contacting the liquid, and thus the DP transducer can always work at its effective temperature range.

The inherent error of this indirect DP measurement approach can be estimated as follows. For each leg of the sub-loop used, the volume of pipe lines is 2.4×10^{-6} m^3, and the volume of the buffer tank is 2.0×10^{-4} m^3. Suppose the liquid PbLi temperature is 300 °C, and the initial argon gas pressure in the sub-loop before liquid PbLi starts to flow is $p_0 = 1.013 \times 10^5$ Pa (this liquid temperature and gas pressure were used in the present experiment). Before the liquid PbLi starts to flow, the valve between the two legs of the sub-loop continually opens so that liquid levels in the two buffer tanks match. After closing this valve and turning on the EM pump to drive the flow of liquid PbLi, both liquid levels in the two buffer tanks are increased. At the steady state, the liquid level in the buffer tank at the upstream H_1 is higher than that at the downstream H_2, and the difference H_1–H_2 causes the measurement error to the pressure drop. From a pressure balance, it can be obtained that:

$$\Delta p = \Delta p' + \rho g (H_1 - H_2), \tag{6}$$

where $\Delta p = p_1 - p_2$ is the real pressure drop to be measured, $\Delta p' = p'_1 - p'_2$ is the reading from DP transducer, and g is the gravitational acceleration. For simplicity, H_2 is assumed to remain zero before and after the PbLi flow is started, and then $p'_2 = p_0$ (although this is not realistic, under this assumption, the estimated error is actually larger than the real one). With this assumption and from the thermodynamics principle, it can be deduced that:

$$p'_1 = \frac{\pi D_{it}^2 H + 9.6 \times 10^{-6}}{\pi D_{it}^2 (H - H_1) + 9.6 \times 10^{-6}} p_0, \tag{7}$$

and then Eq. (6) can be rewritten as:

$$\Delta p = \frac{\pi D_{it}^2 H + 9.6 \times 10^{-6}}{\pi D_{it}^2 (H - H_1) + 9.6 \times 10^{-6}} p_0 - p_0 + \rho g H_1. \tag{8}$$

Based on Eq. (8), H_1 can be obtained for each given Δp value, and the error $\rho g H_1 / \Delta p \times 100\%$ can thus be estimated. The results plotted in Fig. 4 include the measurement errors and the absolute pressure value due to liquid level difference in the two buffer tanks as functions of pressure drop in the MHD PbLi flow. It can be seen that the measurement error decreases with the increase of Δp. Here, the measured pressure drop of MHD PbLi flow's range is 5–75 kPa, and correspondingly, the measurement error's range is 4.0%–2.5%.

Since the idea of using buffer tanks for this indirect DP measurement approach is to decrease the liquid level difference between the two legs, the dimensions (D_{it} and H) of the buffer tank should have influences on the measurement error. This is confirmed by further estimations (with the same assumptions as used before) for different diameters and heights of the buffer tank, as shown in Figs. 5 and 6. Fig. 5 shows that the measurement error decreases sharply when D_{it} is increased from 0.01 m to 0.05 m and only decreases very slightly when D_{it} is increased from 0.05 m to 0.10 m. It indicates that we cannot obtain a continuously decreasing measurement error by enlarging D_{it}. Fig. 6 shows that the height of buffer tank also has a big influence on the measurement error. Smaller H results in smaller measurement error. Note that H discussed here actually represents the initial height of the gas space over the liquid surface before the liquid starts to flow. We only make an assumption here that the initial height of the gas space is equal to the height of buffer tank (the liquid level just reaches to the bottom of buffer tank). In the actual experiments, before the EM

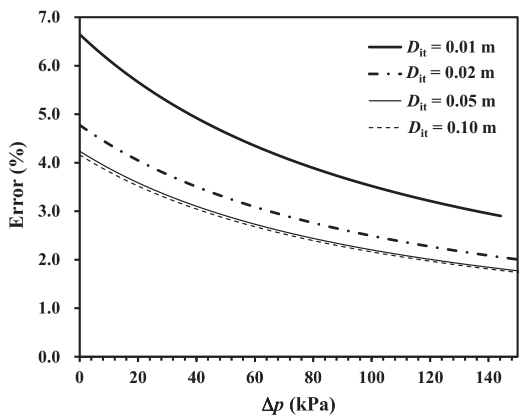

Fig. 5. Influence of inner diameter of the buffer tank on measurement error (with constant $H = 0.047$ m).

pump is turned on to drive the flow in the loop, LM has been partly filled in the buffer tank (only "partly" because the buffer tank is filled with gas beforehand) due to the elevation of liquid surface in the storage tank being higher than the elevation of buffer tank bottom. Therefore, the height of gas space in the buffer tank is smaller than H defined here. This means that the measurement errors in the present experiments are actually smaller than that shown in Fig. 4 for the assumption of $H_2 = 0$ but are reasonably close to that shown in Fig. 6 for the case $H = 0.03$ m. Indeed, during our experiments, the readings from thermocouples set on the outer surface of the buffer tanks have shown the filling-in of liquid PbLi when the flow of PbLi is just started in the loop.

4. Numerical simulation procedures

The fringing magnetic field induces 3D MHD effects on the liquid PbLi flow. Therefore, a fully 3D numerical simulation is necessary for solving the governing equations, as shown in Eqs. (1)–(5), for the problem to be investigated properly. This is accomplished with a 3D parallel code named HIMAG [26] for MHD flows at low magnetic Reynolds number, originally developed by HyPerComp, Inc., in conjunction with UCLA. The HIMAG code utilizes a finite volume scheme to discretize the governing equations with a co-located arrangement of parameters at the cell center. In the momentum equation Eq. (3), the convective and diffusive terms are discretized with a semi-implicit Crank-Nicholson formulation, and a four step projection method is used in the hydrodynamic solver of HIMAG.

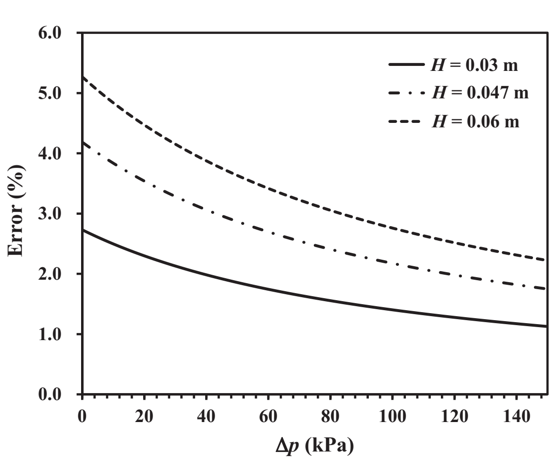

Fig. 6. Influence of height of buffer tank on measurement error (with constant $D_{it} = 0.0732$ m).

The electric potential formulation is utilized for the calculation of magnetic-field-induced electric current density distribution in LM flow.

Simulation meshes are constructed using HIMAG's mesh generator. In the pipe cross section, the mesh is non-uniform in the radial direction while it is uniform in the azimuthal direction. To resolve gradient boundary layers in the liquid at the pipe wall, there are 4 to 5 cells within the distance R_i/Ha from the wall. The mesh size is then geometrically increased inwards toward the axis from there. Axially, the mesh is more refined in the fringing magnetic field region where the gradient of the magnetic field is highest. Overall mesh refinement simulations were performed to ensure the accuracy of our results.

The following boundary conditions are applied: $n \cdot j = 0$ at all outer surfaces, fully developed flow at the inlet, $\partial u/\partial x = 0$ and $p = 0$ at the outlet (where n is the vector normal) and a no-slip condition at the fluid-wall interface.

5. Results and discussions

In the experiments, pressure drops Δp in the liquid PbLi MHD flow at different axial locations were taken between two pressure taps mounted on the tube at a fixed distance of $\Delta L = 0.6$ m. First, the entire test section was centered inside the magnet space so that the middle point of the 0.6 m segment separating the two pressure taps is located at the center of the magnet. After taking measurements of Δp at one axial station, the test section, together with the whole loop, is moved to another station by pulling out the four-wheel carrier from the magnetic field (see Fig. 2). At each station, measurements are carried out for five flow rates and three magnetic field strengths. Each axial displacement is approximately $\Delta x = 0.05$ m. The last measurement is taken at the location where the upstream pressure tap approaches the edge of the fringing magnetic field. As seen from Fig. 1, the total displacement of the upstream pressure tap is 0.7 m, which corresponds to changing its location from its initial position $x = -0.3$ m to $x = -1.0$ m. In the following Figs. 8 and 10–14 showing Δp or pressure gradient as a function of the axial distance, the abscissa x corresponds to the location of the upstream pressure tap relative to the magnetic field center ($x = 0$).

Numerical simulations are then conducted with exactly the same flow conditions as that of the experiments. Apart from data of Δp used for comparisons with experimental measurement and theoretical estimation, detailed velocity fields, pressure distributions, and induced electric current distributions are obtained from the simulations. This detailed information enables deep insights into the mechanism of how the fringing magnetic field induces 3D effects on liquid PbLi MHD flows. For the case of PbLi flow into the magnetic field, the simulated flow domain is 0.8 m long in the streamwise direction (with only one exceptional case of PbLi flow out of the magnetic field, which will be mentioned later), 0.6 m long in the fringing magnetic field and 0.2 m long in the uniform magnetic field region (see Fig. 1, from $x = -1$ m to $x = -0.2$ m). In order to directly compare the simulated Δp with measured data, the pressure distribution up to $x = -0.3$ m (for Δp value at position up to $x = -0.3$ m corresponding to the measurement) has to be supplemented. This is accomplished with extrapolation of the pressure gradient, which in the investigated MHD flow is constant in the uniform magnetic field region.

The flow conditions for different cases investigated in the experiments are listed in Table 1. Some selected cases are numerically simulated. It is seen that the investigated LM PbLi MHD flow has relatively low Hartmann number and high Reynolds number. The maximum magnetic interaction parameter N for the selected numerical simulation cases is only 16.20, indicating that

Table 1
Test cases.

Runs	*Ha* = 108		*Ha* = 215		*Ha* = 322	
	Re	*N*	*Re*	*N*	*Re*	*N*
1	5.40×10^4	0.22	3.23×10^4	1.43	1.83×10^4	5.66
2	4.32×10^4	0.27	2.70×10^4	1.71	1.40×10^4	7.41
3	3.23×10^4	0.36	2.16×10^4	2.14	0.97×10^4	10.69
4	2.16×10^4	0.54	1.62×10^4	2.85	0.64×10^4	16.20
5	1.08×10^4	1.08	1.08×10^4	4.28	0.26×10^4	39.87

the hydrodynamic contribution to pressure drop may be important compared to the electromagnetic contribution as will be seen from the analyses presented later on.

5.1. Pressure drop of MHD PbLi flow in the fringing magnetic field

We begin with comparisons of pressure drops of the liquid PbLi MHD flow in the uniform magnetic field obtained in measurements, numerical simulations, and theoretical estimations. The theoretical estimation of Δp is conducted by using the following equation developed by Miyazaki et al. [27]:

$$\Delta p = L \cdot \frac{c_w}{1 + c_w} \cdot \sigma_f \cdot U \cdot B_0^2, \tag{9}$$

where c_w is the wall conduction ratio defined as $c_w = \sigma_w/\sigma_f \cdot \left(R_o^2 - R_i^2\right) / \left(R_o^2 + R_i^2\right)$ and σ_w is wall conductivity. The results are shown in Fig. 7. It can be seen that the agreement among the experimental, numerical simulation, and theoretical results for the MHD Δp are excellent. It once again testifies the reliability of our indirect Δp measurement technique for high temperature LM MHD flow first demonstrated in [10]. The correctness of numerical simulation results has also been verified from the viewpoint of MHD pressure drop. Note that for the cases at lower *Ha* (Figs. 7(a) and (b)), the simulation results for Δp are slightly higher than those estimated by Eq. (9). This is reasonable since Eq. (9) was derived by neglecting the friction term in the momentum equation of MHD flow, which may contribute to the total Δp in the presently investigated MHD flows at smaller *Ha* but higher *Re* as clearly seen in Figs. 7(a) and (b). Particularly, the measured Δp for the last point at the largest $\mathrm{Re} = 5.4 \times 10^4$ plotted in Fig. 7(a) shows relatively big discrepancy (8%) compared with the estimation by Eq. (9). This should be caused by the omitted contribution of hydrodynamically turbulent friction to the Δp expressed in Eq. (9), since at that large Re but small Ha hydrodynamic turbulence should be still remained in the LM flow. This point will be further explained when showing quantitative analysis of pressure drop in the fringing magnetic field region.

Fig. 8 shows the measured Δp as a function of axial distance in the fringing magnetic field for three Hartmann numbers, together with the numerical simulation results. For the measured MHD flow at each *Ha* two selected typical examples at different Reynolds numbers are presented (others show similar characteristics but are not shown). Theoretical estimations of Δp using Eq. (9) in the uniform magnetic field are also plotted for reference. As seen from Fig. 8, at the highest Hartmann number (*Ha* = 322) of the investigated PbLi pipe flow, experimental and numerical simulation results are in fairly good agreement with each other, with less than a 5% discrepancy. At *Ha* = 215, the agreement between measured Δp and simulation results is still good, with less than a 10% discrepancy. However, at the smallest Hartmann number, big discrepancies between measurement and numerical simulation results are found in the fringing magnetic field region, with maximum discrepancy larger than 30% for the case at *Ha* = 108 and $Re = 4.32 \times 10^4$, as shown in Fig. 8(a1). On the other hand, comparing numerical simulation results with the theoretical estimation for Δp in the uniform magnetic field region, it is seen that they

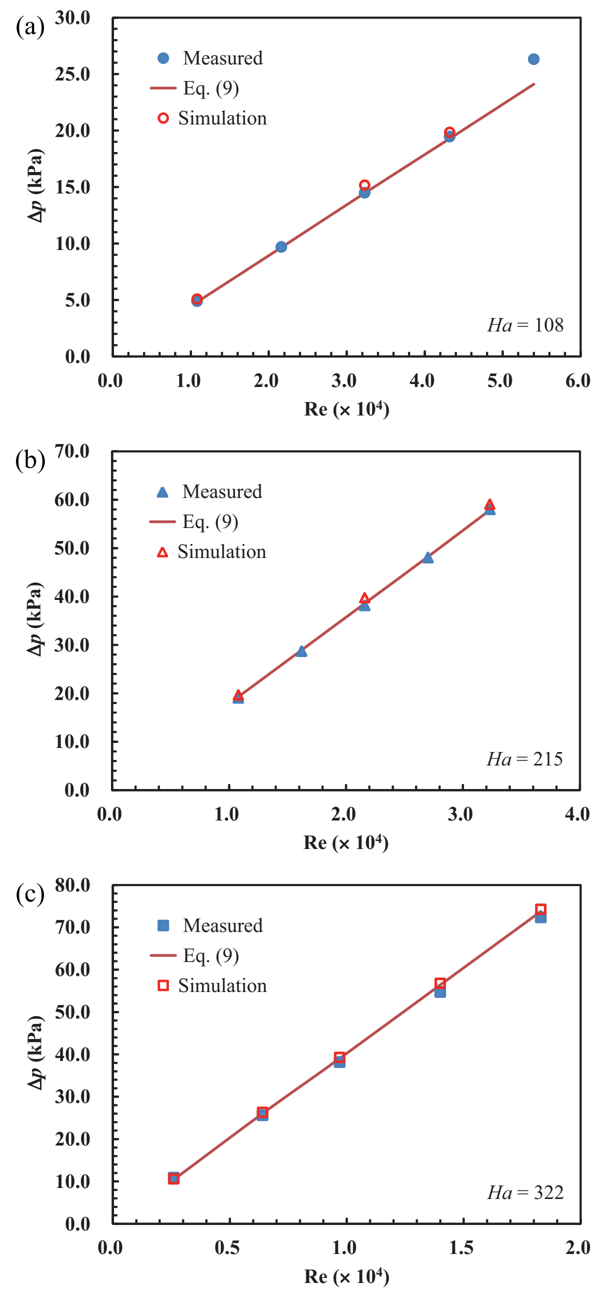

Fig. 7. Comparisons of measured pressure drops with theoretical calculations and numerical simulations at Hartmann numbers (a) *Ha* = 108, (b) *Ha* = 215 and (c) *Ha* = 322.

are in excellent agreement for the cases at *Ha* = 322 but in obvious disagreement for other cases at the two smaller Hartmann numbers, and this disagreement becomes larger with the reduction of *N*. Regarding the abovementioned two types of disagreements, we provide some analyses and explanations next.

The big discrepancy between measurement data and numerical simulation results for Δp in the fringing field region of PbLi MHD flow at small Hartmann but large Reynolds numbers (or similarly, at low interaction parameter *N*) can be attributed mainly to two reasons stemming from both measurement and numerical simulation techniques. The first reason is from the small absolute value of Δp (around 10–20 kPa) for this case. As seen from Figs. 4–6, smaller absolute values of Δp correspond to a larger inherent error for our indirect measurement technique. The second reason is from the

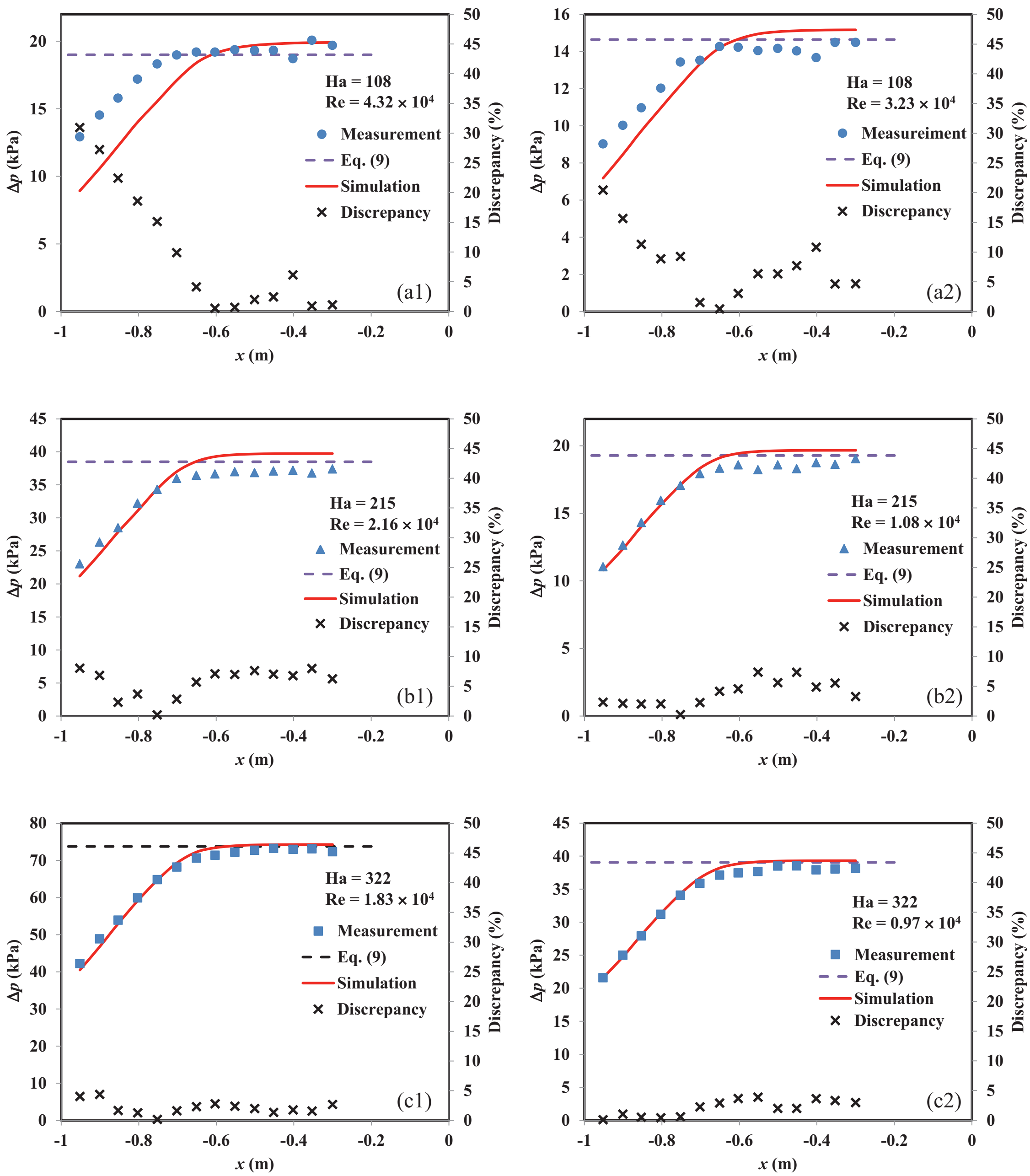

Fig. 8. Distribution of pressure drops of liquid PbLi MHD flow in the fringing magnetic field region for selected flow Reynolds numbers at Hartmann numbers (a) $Ha = 108$, (b) $Ha = 215$ and (c) $Ha = 322$, respectively, together with the discrepancies (discrepancy $= \frac{|\Delta p_{meas} - \Delta p_{num}|}{\Delta p_{meas}} \times 100\%$) between the measured and numerical simulated values.

limitations of the numerical simulation techniques that we used herein. The numerical simulation code HIMAG has been developed specifically for the MHD flows in the environment of nuclear fusion devices, in which all the LM flows are in a laminar state due to the strong MHD effect on suppression of turbulence. In our present experiments, the Reynolds numbers are relatively high for the PbLi flows at $Ha = 108$, at which non-MHD flows are fully turbulent. Since our investigated MHD flow is at the entrance into magnetic field, a turbulent flow state should be maintained for some distance into the fringing region. In numerical simulations using the HIMAG code, a parabolic velocity profile of laminar flow is used as the inlet flow condition, so the skin friction for turbulent flow in the fringing magnetic field present in the experiment has not been taken into account, resulting in a smaller Δp locally as compared with measurements. We take the case shown in Fig. 8(a1) as an example in making a roughly quantitative estimation. For fully turbulent pipe flow, the Blasius equation for the friction factor f is used for estimation where $f = 0.0791 \times Re^{-0.25}$. At $Re = 4.32 \times 10^4$, the contribution of turbulent skin friction force to the LM PbLi flow at the entrance point (within an 0.6-m interval into the fringing magnetic field) is 2.08 kPa, which is about 23% of the HIMAG-simulated value 8.92 kPa, *i.e.*, the discrepancy matches well with that in the figure.

Regarding the uniform magnetic field region, as mentioned previously, one reason for the disagreement between numerical simulation results and the theoretical estimation for Δp (numerical simulation results are slightly higher) at low magnetic interaction parameter is due to the omission of friction force in the deduction of Eq. (9). We can make an estimation of Δp with consideration of

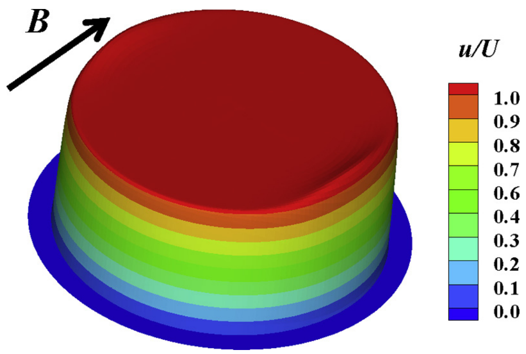

Fig. 9. A typical velocity profile in a cross section of MHD pipe flow in uniform magnetic field region corresponding to the case shown in Fig. 8(b1).

the friction-force contribution, Δp_f, in addition to only the MHD force contribution, Δp_M, obtained by Eq. (9). Δp_f can be written as follows for MHD pipe flow:

$$\Delta p_f = \frac{4L}{D_i} \cdot \bar{\tau_w} = \frac{4L\mu}{D_i} \cdot \left.\frac{\partial \bar{u}}{\partial n}\right|_w, \tag{10}$$

where $\bar{\tau_w}$ and $\partial \bar{u}/\partial n|_w$ are the mean wall shear stress and mean wall-normal velocity gradient at the wall around the pipe inner surface. As shown in Fig. 9 for the typical velocity profile in a cross section of the currently investigated MHD pipe flow in a uniform magnetic field region corresponding to the case plotted in Fig. 8(b1), the velocity profile is of slug type, demonstrating a uniform core region and a variable thickness boundary layer with the minimal thickness of R_i/Ha at the point where the magnetic field is perpendicular to the wall. Hence, the wall normal velocity gradient computed at this point can be taken to estimate Δp_f. For this example, the estimated Δp_f is 0.76 kPa, and Δp_M based on Eq. (9) shown in Fig. 8(b1) is 38.57 kPa. And so the corrected Δp is 39.33 kPa as compared with the numerical simulation result 39.74 kPa. Nevertheless, Eq. (9), in spite of the omitted friction-force contribution, has been fairly accurate even for MHD LM flow at high Reynolds number as presently investigated. The discrepancy between the estimated Δp based on Eq. (9) and numerical simulation result is only 2.9%.

For the estimation of pressure drop in LM MHD flow in a strong fringing magnetic field region, Miyazaki et al. [22] proposed a simple integral of pressure gradient along the fringing field based on their experimental results for a MHD NaK flow:

$$\Delta p = \frac{c_w}{1+c_w} \int \sigma_f U B^2 dx. \tag{11}$$

For a steady LM flow at constant temperature, Eq. (11) becomes:

$$\Delta p = \frac{c_w}{1+c_w} \cdot \sigma_f \cdot U \cdot \int B^2 dx. \tag{12}$$

Based on our numerical simulation results for PbLi MHD flows in a fringing magnetic field, we have verified this approach. Using Eqs. (1) and (12), Δp within an interval of 0.6 m in the streamwise direction is estimated and compared with the numerical simulation results. Only the flows at $Ha = 322$ are chosen for comparisons because for other two experimental values of the Hartmann number the magnetic field cannot be considered as strong enough for using Eq. (12), *i.e.*, the friction-force contribution to the pressure gradient is not negligible (Fig. 8). As shown in Fig. 7, the estimated values of Δp in the fringing magnetic field region for all the five flows at different Reynolds

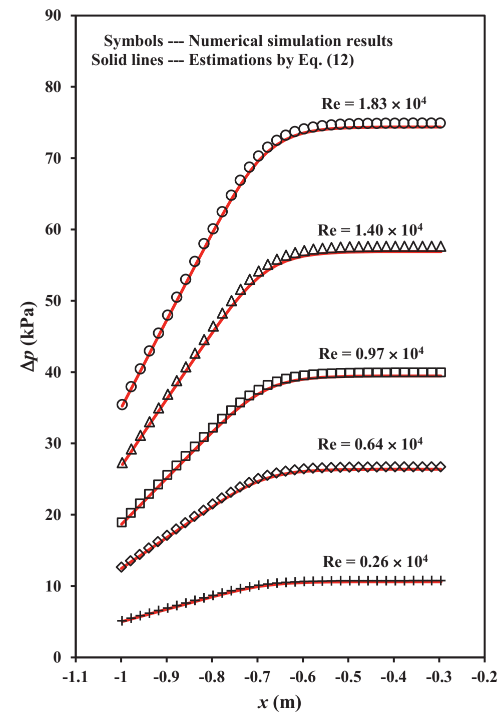

Fig. 10. Comparisons of the estimated pressure drops in fringing magnetic field using Eqs. (1) and (12) with numerical simulation results for PbLi MHD flows at $Ha = 322$.

numbers by the simple integral Eq. (12) are in excellent agreement with the numerical simulation results. This excellent agreement indicates that the simple approach for estimation of pressure drop in LM MHD flow in a fringing magnetic field with quasi-fully-developed MHD flow assumptions is accurate at least at the investigated Hartmann number, $Ha = 322$. The effective ranges of Hartmann number and/or magnetic interaction parameter for this conclusion need to be defined by further systematic studies.

Although the pressure drop (gross flow feature) can be accurately estimated with quasi-fully-developed MHD flow assumptions as shown in Fig. 10, the fringing magnetic field generates 3D effects on local characteristics of the flow. In terms of the axial pressure gradient, it can be locally different around the magnet pole front edge when measured on the walls perpendicular ($\left(\mathrm{d}p/\mathrm{d}x\right)_H$) and parallel ($\left(\mathrm{d}p/\mathrm{d}x\right)_S$) to the magnetic field, respectively, as reported in [20,21]. As shown in Fig. 11, within the presently simulated Ha (or N) range, the difference between profiles of $\left(\mathrm{d}p/\mathrm{d}x\right)_H$ and $\left(\mathrm{d}p/\mathrm{d}x\right)_S$ is not obvious by direct comparison. In order to exaggerate the difference between the profiles of $\left(\mathrm{d}p/\mathrm{d}x\right)_H$ and $\left(\mathrm{d}p/\mathrm{d}x\right)_S$, $\left(\mathrm{d}p/\mathrm{d}x\right)_H - \left(\mathrm{d}p/\mathrm{d}x\right)_S$ is calculated and also shown in Fig. 11. In doing so, the 3D effect of a fringing magnetic field on MHD PbLi flow becomes evident, *i.e.*, the pressure gradient taken on the wall perpendicular to the magnetic field is obviously different from that taken on the wall parallel to the field, and this difference happens around the magnet pole edge at $x = -0.7$ m. $\left(\mathrm{d}p/\mathrm{d}x\right)_H$ is equal to $\left(\mathrm{d}p/\mathrm{d}x\right)_S$ at the entrance of the fringing magnetic field and gradually the former becomes smaller than the latter as LM flows downstream, and a peaked structure appears on the profile of $\left(\mathrm{d}p/\mathrm{d}x\right)_H - \left(\mathrm{d}p/\mathrm{d}x\right)_S$ before the magnet pole front edge. After the pole edge, $\left(\mathrm{d}p/\mathrm{d}x\right)_H$ becomes larger than $\left(\mathrm{d}p/\mathrm{d}x\right)_S$ and another peaked structure appears on the profile of $\left(\mathrm{d}p/\mathrm{d}x\right)_H - \left(\mathrm{d}p/\mathrm{d}x\right)_S$

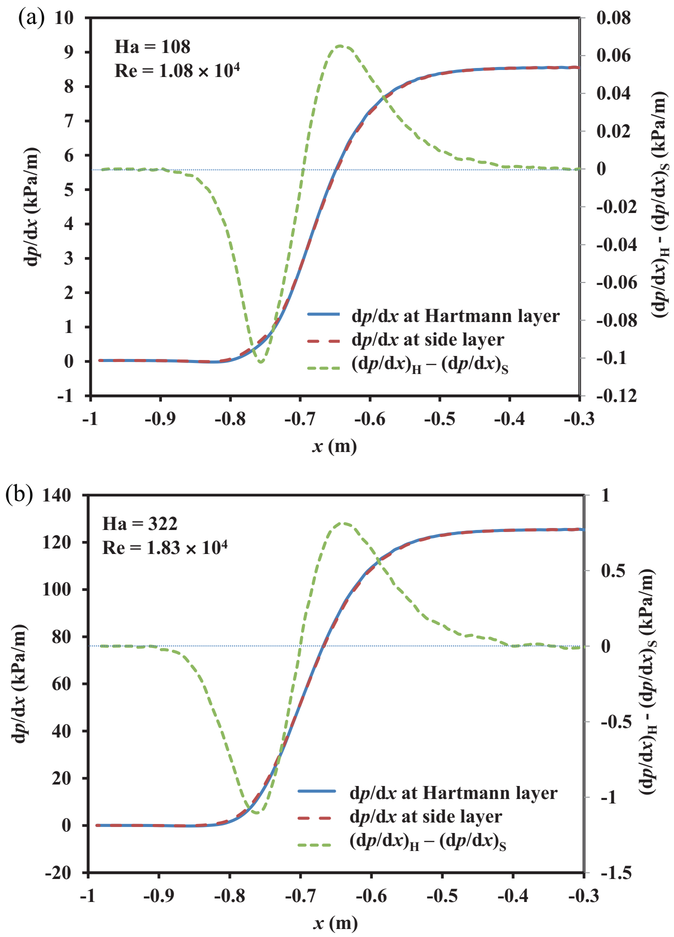

Fig. 11. Comparisons of axial pressure gradients in liquid PbLi MHD flow taken at the Hartmann layer and side layer, respectively, for two selected examples of numerical simulations at (a) $Ha = 108$, $Re = 1.08 \times 10^4$ and (b) $Ha = 322$, $Re = 1.83 \times 10^4$.

after which $(\mathrm{d}p/\mathrm{d}x)_H$ becomes equal to $(\mathrm{d}p/\mathrm{d}x)_S$ again when the flow enters into the uniform magnetic field region.

5.2. Comparisons between LM MHD flows entering and leaving the magnetic field

So far, the reported studies, both experimental and numerical, on LM MHD flow in a circular tube in a transverse non-uniform magnetic field were almost all for the case of exiting flow, *i.e.*, LM flows out the magnetic field region. In [22] only, an experiment on MHD pressure drop of NaK flow in a circular duct was reported for the case of flow entering a fringing magnetic field as well as the case of flow exiting the field. No significant difference in pressure drop was seen in the measurement data between the inlet and outlet fringing field cases [22]. In [28], the authors studied the effects of a fringing magnetic field on a MHD flow in a rectangular duct by numerical simulations. Both cases of MHD flows entering and exiting a fringing magnetic field were simulated. Some differences regarding flow structures and unbalanced pressure distributions in the cross section of the duct were found for these two cases. In order to make a comparison between liquid PbLi MHD flow in a circular pipe entering and flowing out the magnetic field, an additional numerical simulation is performed on a PbLi flow exiting a transverse fringing magnetic field in a range from $x = 0$ to $x = 1$ m (x corresponds to the coordinate shown in Fig. 1). The profile of the fringing magnetic field is the right part shown in Fig. 1. The case of PbLi MHD flow at $Ha = 215$ and $Re = 2.16 \times 10^4$ is simulated.

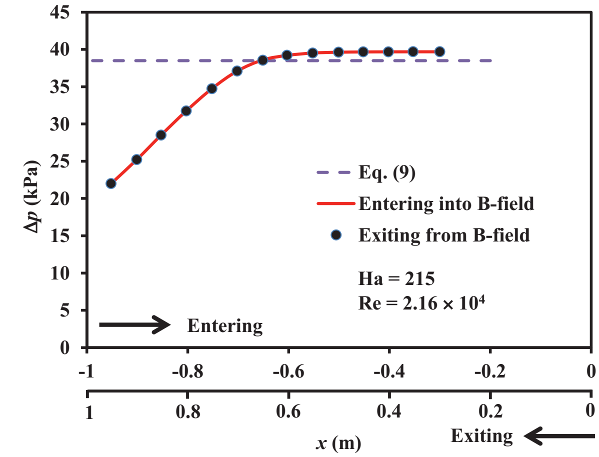

Fig. 12. MHD pressure drops in fringing magnetic field for the two cases of LM flowing into and out of the magnetic field, respectively.

As shown in Fig. 12, for MHD pressure drop, there is no visible difference at the same relative position (*e.g.*, same distance from the center of magnetic field), which is in agreement with that reported in the experiment [22]. For the axial pressure gradient, the profiles of $(\mathrm{d}p/\mathrm{d}x)_H - (\mathrm{d}p/\mathrm{d}x)_S$ for both cases vary differently in the flow direction, as shown in Fig. 13. For the MHD flow at the entrance into the fringing magnetic field, the profile of $(dp/dx)_H - (dp/dx)_S$ reaches at first a negative peak in front of the magnet pole edge, and then reaches another positively peaked structure after passing the pole edge. For the case of MHD flow

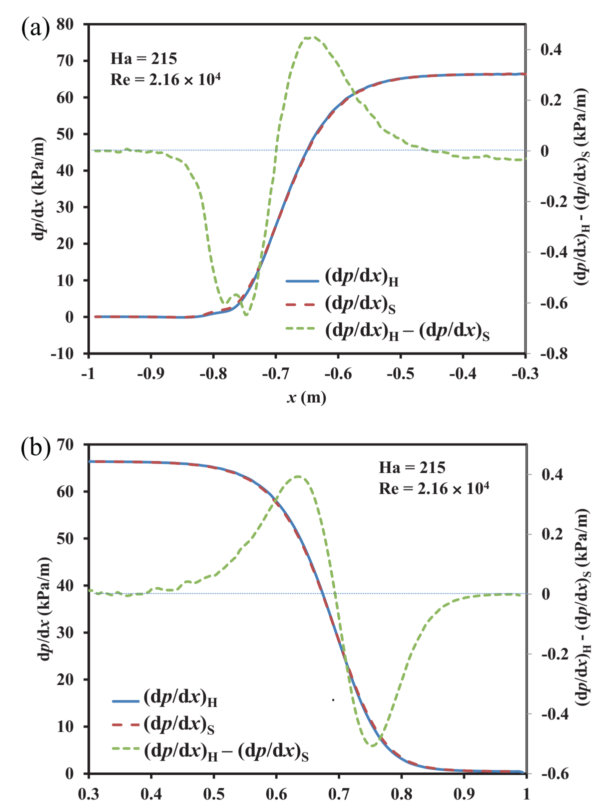

Fig. 13. Comparisons of axial pressure gradients in a fringing magnetic field for the two cases of LM flowing (a) into and (b) out of the magnetic field.

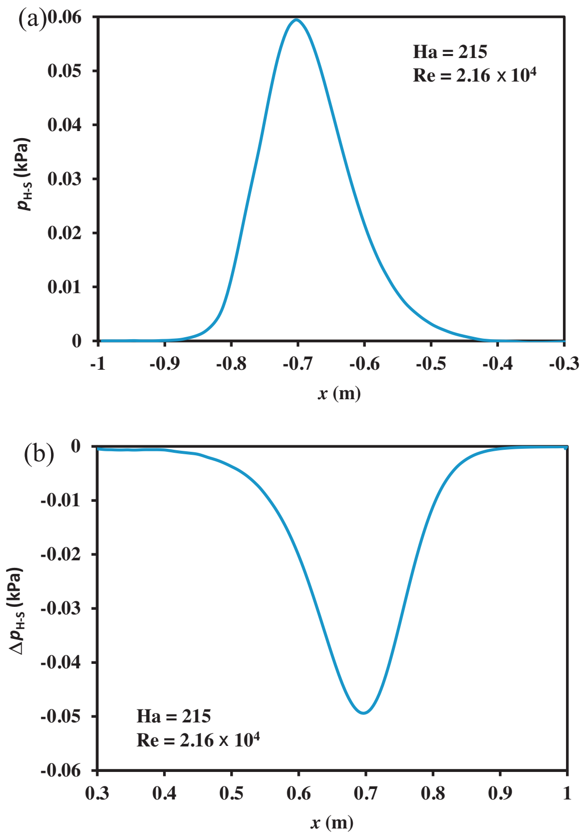

Fig. 14. Comparisons of pressure differences between locations adjacent to the Hartmann wall and side wall for the two cases of LM flowing (a) into and (b) out of the magnetic field.

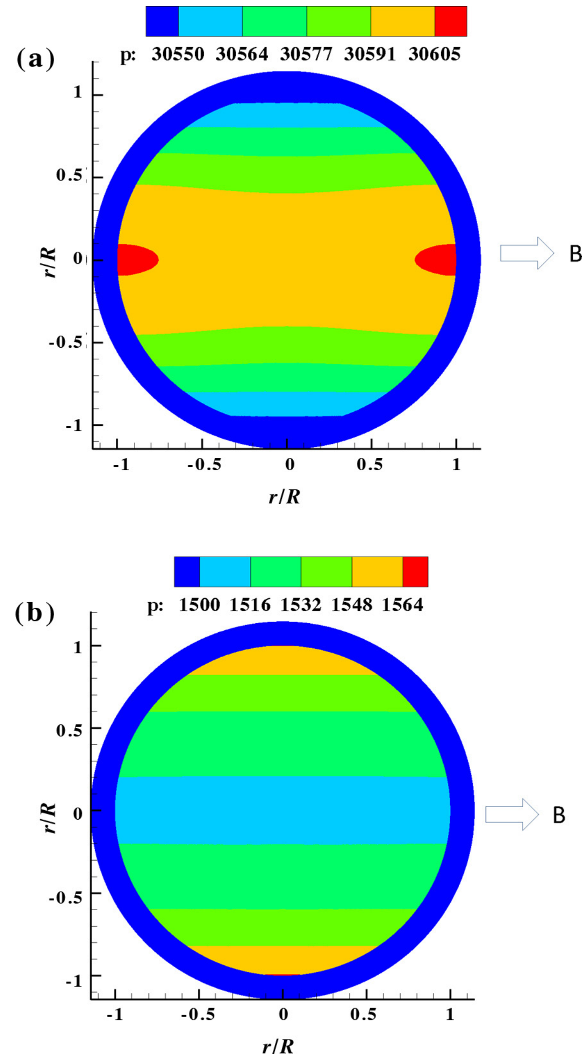

Fig. 15. Comparisons of pressure distributions in a cross section of flow duct at the magnet pole edge locations $x = \pm 0.7$ m for the two cases of LM flowing (a) into and (b) out of the magnetic field.

exiting the magnetic field, the positive peak appears at first in the profile of $\left(\mathrm{d}p/\mathrm{d}x\right)_H - \left(\mathrm{d}p/\mathrm{d}x\right)_S$ before reaching the magnet pole edge and then the negatively peaked structure after the pole edge. However, if we look at this phenomenon from the viewpoint of relative position in the magnetic field, the phenomena appearing in the profiles of $\left(\mathrm{d}p/\mathrm{d}x\right)_H - \left(\mathrm{d}p/\mathrm{d}x\right)_S$ for both cases are the same, *i.e.*, the positively peaked structure appears in between the uniform magnetic field region and the magnet pole edge, and the negative one appears outside the magnet pole edge.

The 3D effect induced by the transverse fringing magnetic field on a LM MHD flow also appears in the non-uniform pressure distribution, *i.e.*, the non-zero transverse pressure difference between the pressures taken at the walls perpendicular and parallel to the magnetic field, Δp_{H-S}, in a cross section of the flow passage at a location around the magnet pole front edge, as already reported in [21,23,24]. However, it can be seen from our numerical simulations that the non-zero transverse pressure differences Δp_{H-S} in the fringing magnetic field region for the two cases of LM flow entering and leaving the magnetic field have different values. As shown in Fig. 14, around the magnet pole edge, the pressure at the wall perpendicular to the magnetic field is higher than that at the wall parallel to the magnetic field for the case of LM flow entering the magnetic field region, resulting in a positively peaked structure in the profile of Δp_{H-S} (Fig. 14(a)), while it is opposite for the case of flow exiting the magnetic field, resulting in a negatively peaked structure on the profile of Δp_{H-S} around the magnet pole edge (Fig. 14(b)).

The non-uniform pressure distribution in the duct cross section located in the fringing magnetic field, corresponding to the magnet pole edge ($x = 0.7$ m), is shown in Fig. 15 more clearly. For both cases of flowing into and out of the magnetic field, there is a pressure gradient in the direction normal to the applied transverse magnetic field in the cross section. The difference is that the pressure gradient is oriented from the central region to the walls parallel to the magnetic field for the entering flow case (with the maximum pressure value located at the Hartmann wall, Fig. 15(a)), while the direction of pressure gradient is opposite for the exiting flow case (with the maximum pressure value located at the side wall, Fig. 15(b)). Since the local 3D effect caused by a fringing magnetic field on MHD LM flow is due to the induced electric current (particularly the axial component, j_x) and the Lorentz force in the liquid, this difference appearing in the non-uniform pressure distributions in both cases can be explained by the different induced electric current distributions, as shown in Fig. 16 for the contour map of j_x and streamlines of induced electric current in the central plane normal to the magnetic field. Note that although streamlines are distributed everywhere in this central plane, the j_x component with large absolute value is strictly limited to the center of the circular duct and around the magnet pole edge. Fig. 16(b) is for the case of LM flowing out of the magnetic field, showing that the induced electric current is mostly parallel to the flow direction in the upper half of the flow domain but opposite to the flow direction in the lower half of the flow domain. The left-hand rule states that the Lorentz force component caused by the axial electric current component

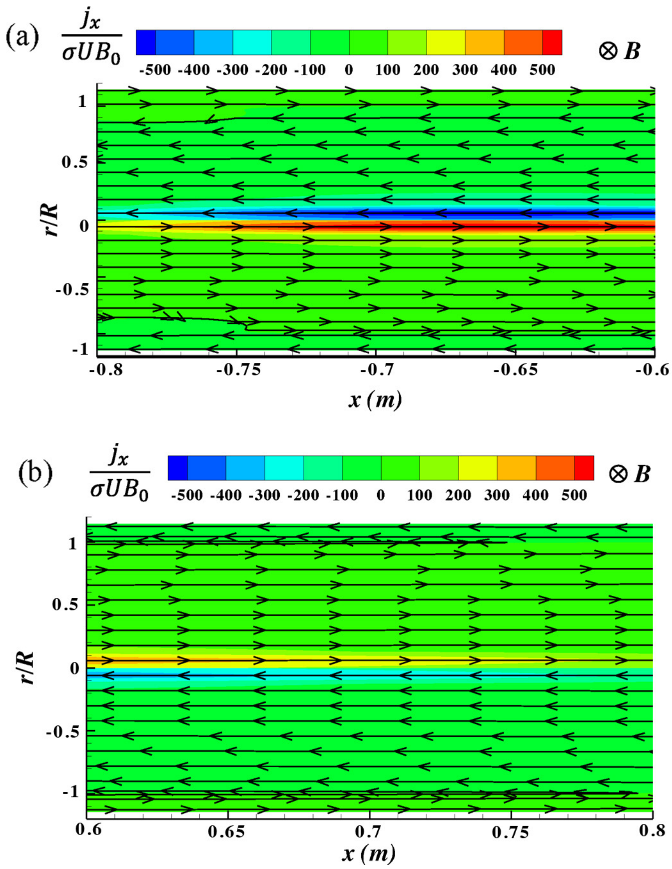

Fig. 16. Comparisons of induced electric current distributions in the central plane normal to the magnetic field for the two cases of LM flowing (a) into and (b) out of the magnetic field.

is in the direction pointing to the walls parallel to the magnetic field and pushes fluid to those walls, resulting in the highest local fluid pressure (Fig. 15(b) and Fig. 14(b)). On the contrary, for the case of LM flowing into the magnetic field, Fig. 16(a) shows that the induced electric current is in opposite directions in the upper and lower half of flow domains as compared with the case shown in Fig. 16(b). Consequently, the corresponding Lorentz force component is normal to the applied magnetic field but points to the center of the flow domain and pulls fluid away from the walls parallel to the magnetic field and pushes it to the center region, resulting in the lowest fluid pressure locally adjacent to those walls (Fig. 15(a) and Fig. 14(a)).

Similar tendencies were observed in a study of 3D MHD flows in a non-conducting rectangular duct in a fringing magnetic field [29]. Namely, it was found that the pressure and velocity distributions in the flow were different between the entry and exit zones of the magnet. Also, a significant difference between the pressure at the Hartmann wall and that at the side wall was found. Similar to the present study, this difference increases as the interaction parameter is increased. However, the 3D effects observed in [29] seem to be stronger compared to those in the present study, probably due to different geometry, different flow parameters used in [29] and also due to the fact that in the experiments in [29] the duct was non-conducting while a conducting pipe is used in the present study.

6. Conclusions

Experiments and 3D numerical simulations of molten PbLi MHD flow in a circular duct under non-uniform transverse magnetic field have been carried out in order to establish a reliable approach for measuring pressure drop in a high-temperature LM MHD flow as well as to investigate the MHD characteristics of molten PbLi flow influenced by a fringing magnetic field. The main conclusions drawn from this study are as follows:

(1) The proposed indirect approach for measuring pressure drop of high temperature LM flow using normal differential pressure sensors for gas flow demonstrates adequate measurement accuracy. The inherent measurement error of this indirect approach decreases with the increase of differential pressure to be measured, increase of the buffer tank diameter, and the decrease of the buffer tank height.

(2) At the investigated Hartmann number, $Ha = 322$, the simple integral equation based on the quasi-fully-developed MHD flow assumption is suitable for estimating the pressure drop in LM MHD flow in a fringing magnetic field. The effective ranges of Hartmann number and/or magnetic interaction parameter for its suitability need to be defined by further studies.

(3) For the two cases of LM flow entering and exiting the magnetic field, the pressure distributions in the flow duct cross section at the axial location around the magnet pole edge are non-uniform. And the non-uniform pressure distribution patterns for these two cases are different: for the case of flow entering the magnetic field, the fluid pressure adjacent to the wall perpendicular to the magnetic field is higher than that adjacent to the wall parallel to the magnetic field, while it is opposite for the other case. This difference is caused by the different induced electric current distributions for the two cases.

Acknowledgements

We appreciate the assistance from Tomas Sketchley and Jonathan Burris of UCLA on operating PbLi MHD flow experiments and from Peter Huang of HyPerComp, Inc., on performing numerical simulations.

References

[1] S. Malang, M. Tillack, C.P.C. Wong, N. Morley, S. Smolentsev, Development of the lead lithium (DCLL) blanket concept, Fusion Sci. Technol. 60 (2011) 249–256.
[2] G. Rampal, A. Li Puma, Y. Poitevin, E. Rigal, J. Szczepanski, C. Boudot, HCLL TBM for ITER-design studies, Fusion Eng. Des. 75–79 (2005) 917–922.
[3] L. Giancarli, L. Baraer, P. Leroy, J. Mercier, E. Proust, Y. Severi, et al., Water-cooled lithium-lead blanket design studies for DEMO reactor: definition and recent developments of the box-shaped concept, Fusion Technol. 21 (1992) 2081–2088.
[4] H.U. Borgstedt, G. Frees, G. Drechsler, Corrosion of stainless steel in flowing PbLi eutectic, J. Nucl. Mater. 141–143 (1986) 561–565.
[5] F. Barbier, Continuous monitoring and adjustment of the lithium content in liquid Pb-Li alloys: assessment of an electrical resistivity meter in a loop system, Fusion Eng. Des. 36 (1997) 299–308.
[6] Main Facilities in ENEA, http://web.brasimone.enea.it/mat/matindfa.htm
[7] I. Bucenieks, R. Krishbergs, E. Platacis, G. Lipsbergs, A. Shishko, A. Zik, et al., Investigation of corrosion phenomena in EUROFER steel in Pb-17Li stationary flow exposed to a magnetic field, Magnetohydrodynamics 42 (2006) 237–251.
[8] Q.-Y. Huang, M.-L. Zhang, Z.-Q. Zhu, S. Gao, Y.-C. Wu, Y.-F. L., et al., the FDS Team, Corrosion experiment in the first LM LiPb loop of China, Fusion Eng. Des. 82 (2007) 2655–2659.
[9] J.S. Yoon, D.W. Lee, Y.D. Bae, S.K. Kim, K.S. Jung, S. Cho, Development of an experimental facility for a liquid breeder in Korea, Fusion Eng. Des. 86 (2011) 2212–2215.
[10] S. Smolentsev, F.-C. Li, Y. Ueki, N. Morley, M. Abdou, T. Sketchley, Construction and initial operation of MHD PbLi facility at UCLA, Fusion Eng. Des. 88 (5) (2013) 317–326.
[11] M.G. Barker, D.J. Siddons, F. Barbier, The removal of nickel dissolved in Pb-17Li by the formation of a less soluble nickel-manganese alloy, J. Nucl. Mater. 233–237 (1996) 1436–1440.
[12] G. Benamati, C. Fazio, I. Ricapito, Mechanical and corrosion behaviour of EUROFER 97 steel exposed to Pb-17Li, J. Nucl. Mater. 307–311 (2002) 1391–1395.
[13] J. Konys, W. Krauss, Z. Voss, O. Wedemeyer, Comparison of corrosion behavior of bare and hot-dip coated EUROFER steel in flowing Pb-17Li, J. Nucl. Mater. 367–370 (2007) 1144–1149.

[14] J. Konys, W. Krauss, J. Novotny, H. Steiner, Z. Voss, O. Wedemeyer, Compatibility behavior of EUROFER steel in flowing Pb-17Li, J. Nucl. Mater. 386–388 (2009) 678–681.
[15] R. Krishbergs, E. Ligere, F. Muktepavela, E. Platacis, A. Shishko, A. Zik, Experimental studies of the strong magnetic field action on the corrosion of RAFM steels in Pb17Li melt flows, Magnetohydrodynamics 45 (2009) 289–296.
[16] J. Konys, W. Krauss, H. Steiner, J. Novotny, A. Skrypnik, Flow rate dependent corrosion behavior of Eurofer Steel in Pb-15.7Li, J. Nucl. Mater. 417 (2011) 1191–1194.
[17] P. Hubberstey, T. Sample, Thermodynamic and experimental evaluation of the sensitivity of Pb-17Li breeder blankets to atmospheric contamination, J. Nucl. Mater. 191–194 (1992) 277–282.
[18] I. Ricapito, A. Ciampichetti, G. Benamati, Pb-17Li/water interaction in DEMO WCLL blanket: water micro-leaks, Fusion Eng. Des. 65 (2003) 577–587.
[19] A. Ciampichetti, I. Ricapito, A. Aiello, G. Benamati, Water large leaks into liquid Pb-17Li: first experimental results on LIFUS 5 facility, Fusion Eng. Des. 69 (2003) 563–567.
[20] B.F. Picologlou, C.B. Reed, P.V. Dauzvardis, Experimental and analytical investigations of magnetohydrodynamic flows near the entrance to a strong magnetic field, Fusion Technol. 10 (1986) 860–865.
[21] C.B. Reed, B.F. Picologlou, T.Q. Hua, J.S. Walker, ALEX results – A comparison of measurements from a round and a rectangular duct with 3-D code predictions, in: Proceedings of 12th Symposium on Fusion Engineering, Monterey, CA, October 12–16, 1987.
[22] K. Miyazaki, K. Konishi, S. Inoue, MHD pressure drop of LM flow in circular duct under variable transverse magnetic field, J. Nucl. Sci. Technol. 28 (1991) 159–161.
[23] X. Albets-Chico, H. Radhakrishnan, S. Kassinos, B. Knaepen, Numerical simulation of a liquid-metal flow in a poorly conducting pipe subjected to a strong fringing magnetic field, Phys. Fluids 23 (2011) 047101.
[24] M.-J. Ni, R. Munipalli, N. Morley, P. Huang, M. Abdou, Validation case results for 2D and 3D MHD simulations, Fusion Sci. Tech. 52 (2007) 587–594.
[25] J. Takeuchi, S. Satake, T. Kunugi, T. Yokomine, N.B. Morley, M.A. Abdou, Development of PIV technique under magnetic fields and measurement of turbulent pipe flow of FLiBe simulant fluid, Fusion Sci. Tech. 52 (2007) 860–864.
[26] R. Munipalli, S. Shankar, M.-J. Ni, N.B. Morley, Development of a 3-D incompressible free surface MHD computational environment for arbitrary geometries: HIMAG, DOE SBIR Phase-II Final Report (2003).
[27] K. Miyazaki, S. Kotake, N. Yamaoka, S. Inoue, Y. Fujii-E, MHD pressure drop of NaK flow in stainless steel pipe, Nuclear Tech./Fusion 4 (1983) 447–452.
[28] T. Zhou, H.-L. Chen, Z.-Y. Yang, Effect of fringing magnetic field on magnetohydrodynamic flow in rectangular duct, Fusion Eng. Des. 86 (2011) 2352–2357.
[29] A.V. Tananaev, Flows in Ducts of MHD Devices, Atomizdat, Moscow, 1979 (in Russian).